New Journal of Physics
The open access journal at the forefront of physics

Deutsche Physikalische Gesellschaft DPG
IOP Institute of Physics

Published in partnership with: Deutsche Physikalische Gesellschaft and the Institute of Physics

OPEN ACCESS

RECEIVED
17 December 2020

REVISED
25 February 2021

ACCEPTED FOR PUBLICATION
19 March 2021

PUBLISHED
7 April 2021

PAPER

Generation of high-quality GeV-class electron beams utilizing attosecond ionization injection

Zsolt Lécz[1,*], **Alexander Andreev**[1,2], **Christos Kamperidis**[1] **and Nasr Hafz**[1,3,4]

[1] ELI-ALPS, ELI-HU Non-Profit Ltd., Wolfgang Sandner utca 3, Szeged, H-6728, Hungary
[2] Nonlinear optics and short pulse spectroscopy, Max-Born Institute, Berlin, Germany
[3] Laboratory on High Power Laser and Physics, SIOM, Shanghai 201800, China
[4] Department of Plasma and Nuclear Fusion, Nuclear Research Center, Atomic Energy Authority, Abu-Zabal 13759, Egypt
[*] Author to whom any correspondence should be addressed.

E-mail: zsolt.lecz@eli-alps.hu

Keywords: relativisitc electron beam, mono-energetic electron beam, low emittance, laser wave-guide, ionization injection, laser wakefield acceleration

Abstract

Acceleration of electrons in laser-driven plasma wakefields has been extended up to the 10 GeV energy within a distance of 10s of centimeters. However, in applications, requiring small energy spread within the electron bunch, only a small portion of the bunch can be used and often the low-energy electrons represent undesired background in the spectrum. We present a compact and tunable scheme providing clean and mono-energetic electron bunches with less than one percent energy spread and with central energy on the GeV level. It is a two-step process consisting of ionization injection with attosecond pulses and acceleration in a capillary plasma wave-guide. Semi-analytical theory and particle-in-cell simulations are used to accurately model the injection and acceleration steps.

1. Introduction

Recent advances in particle accelerators using some state-of-the art laser-plasma acceleration techniques has proven that such technologies are capable of generating high-energy electron bunches in the GeV (giga-electronvolt) energy range [1–6] in a table-top environment using high power lasers [7, 8]. The mechanism allowing such acceleration technique is called laser wakefield acceleration naturally present in underdense gaseous plasma medium, where the electron plasma frequency is much lower than the laser frequency [9, 10]. The electron's high energy itself is often demanded, but in several advanced applications also the electron beam quality has to meet strict requirements. Such key parameters are the transverse emittance and energy spread within the bunch, which have to be as low as possible for a successful transportation of the electron bunch through magnetic devices, especially in the case of coherent x-ray radiation emission.

The first crucial step in achieving quasi mono-energetic electron beams is the electron injection mechanism, because the final beam energy spread is strongly related to the initial one during the injection process into the wakefield. In the last two decades several injection mechanisms have been proposed and experimentally realized [11–17]. For low charge, but well-controlled injection, the ionization injection is used recently [18, 19], which can provide very small energy spread in a two-color laser scheme, which requires two laser pulses with different frequencies [20–22]. A significant reduction of the energy spread was achieved by using nano-droplets [23, 24]. Very short electron bunches can be injected if a sharp transition is introduced in the density distribution of the background gas by different means [25–27], or by triggering the plasma wavebreaking via tight focusing of the laser pulse [28, 29]. Significant effort has been put into the electron-beam-driven wakefield acceleration [30–33], where the phase velocity of the plasma wave is basically constant during the acceleration. This is a great advantage of highly relativistic electron beams in contrast to the laser pulses, where the problem of dephasing always arises.

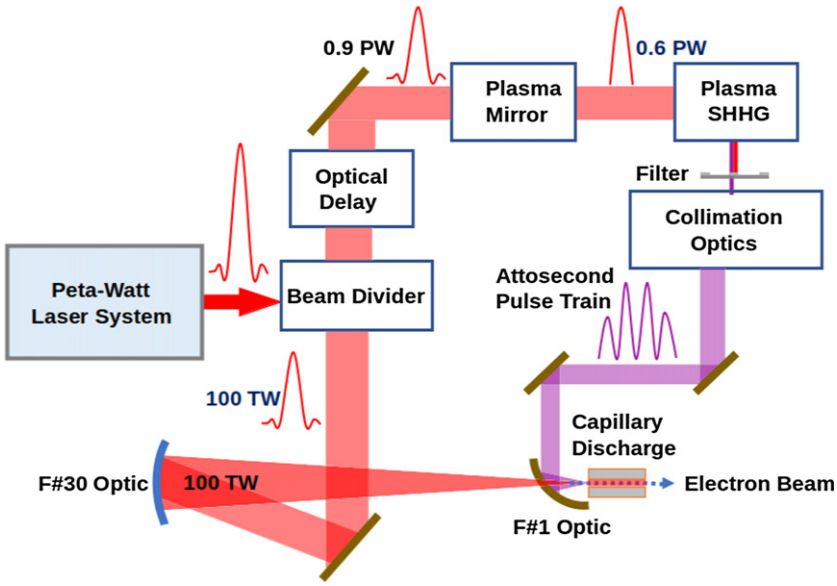

Figure 1. Proposed experimental setup.

In this work we propose a new method to generate GeV electron bunches with less than 1% energy spread using a two-color injection scheme in a capillary discharge plasma waveguide, which allows the guidance of a laser pulse with an average power of the order of 100 TW and with total energy of several Joules. The very small energy spread is provided by the ionization injection induced by intense attosecond pulses focused at the right position behind the driving pulse to a focal spot smaller than 1 μm [21]. A Peta-Watt laser pulse, with 20 J total energy, is split into two parts (see Figure 1): the first one is used to generate a train of intense attosecond pulses (atto-pulses) via surface high harmonic generation (SHHG) and the second is used to drive the wakefield acceleration. The first pulse will generate high harmonics via the relativistic oscillating mirror mechanism [34] and the low frequency components (below the 3rd harmonic) will be filtered out. The remaining pulses have a central wavelength of 114 nm (7th harmonic) and they are focused to a 0.3 micron spot size near the entrance of a 15 mm long capillary waveguide. The gas is a mixture of any gas with low ionization potential with ~1–10% Neon. After applying the discharge current in the capillary plasma a parabolic density profile will evolve with an electron density of $n_0 = 6 \times 10^{17}$ cm^{-3} on axis [35, 36].

The atto-pulses have to ionize Ne^{9+} and Ne^{10+}, therefore their intensity at focus should be larger than $I_{th} = 2 \times 10^{19}$ W cm^{-2}. The intensity of the generating laser pulse is above 10^{21} W cm^{-2}, which should be sufficient to achieve the desired intensity of the atto-pulses, since the conversion efficiency for these harmonics is well above 1 percent [37–39]. The second laser pulse has a peak intensity slightly smaller than I_{th}, i.e. below the ionization threshold of Ne^{9+}. The electron bunch will be injected at the beginning of the interaction and, in proper conditions, its energy spread remains below 10 MeV after 1 cm distance.

2. Ionization of neon with attosecond pulse train

The low level ionization states (from 1 to 8) of neon are produced by the driving pulse, which propagates in front of the atto-pulse train with an optimum temporal separation, to be defined later. It is important to note that the duration of each pulse is 300 as, which is much longer than the atomic time scale for ionization of inner shell electrons [40]: $\hbar/U_i \approx 0.5$ as, where $\hbar$ is the Planck's constant and $U_i \sim 1$ keV is the ionization potential. The Keldysh parameter [41] in our case is smaller than unity: $\gamma_k = \sqrt{U_i/2U_p} \sim 0.1$, where $U_p = e^2E_L^2/(4m_e\omega_L^2)$ is the ponderomotive potential. Therefore the tunneling, or barrier suppression, ionization is the main mechanism responsible for the electron injection [42], which is implemented in the code used for our simulations, EPOCH [43].

The focused attosecond pulses are simulated in 2D geometry propagating in a uniform density plasma which contains Neon ions. The intensity of the pulses and the generated electrons are shown in figures 2(a)–(c). The peak intensity of the pulses is $I_a = 8 \times 10^{19}$ W cm^{-2}. One can see that ionization occurs only within the Rayleigh length of the pulses, which is $l_R \approx 3$ μm. The number of electrons released from ionization in figure 2 is around 30 000, which means about 0.005 pC for 1% density ratio of neon. We note here that the focal spot diameter of the attopulses in figure 2 is only 0.6 μm. The number of injected

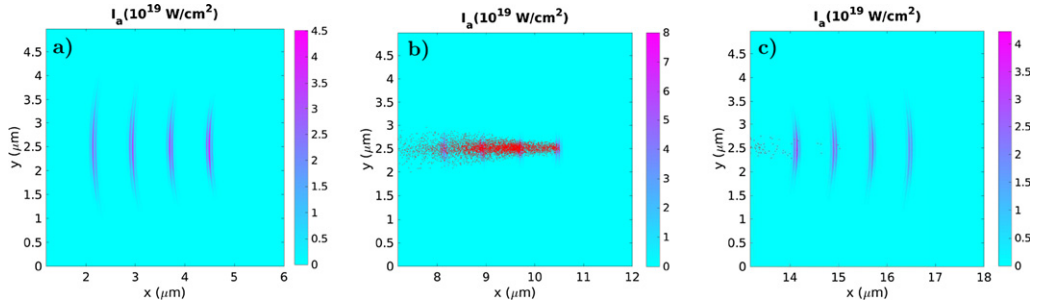

Figure 2. Color scale shows the intensity distribution of the pulse train, while the red dots corresponds to electrons released from Ne^{9+} and Ne^{10+}.

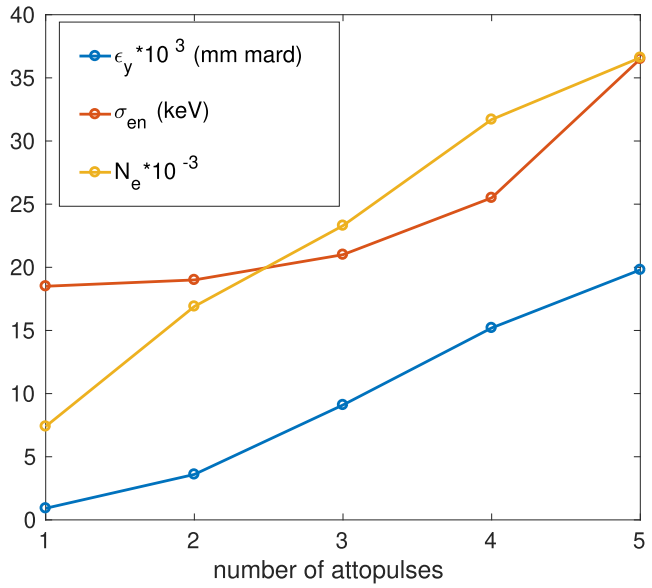

Figure 3. Parameters of the electron bunch right after the ionization as a function of number of attopulses. The emittance is multiplied by 1000 and the number of electrons is divided by 1000 in order to show these curves in one frame.

electrons can be easily controlled by changing the focal spot diameter of the pulses or by changing the relative density of neon. The total energy in the attopulse train, with 1% SHHG efficiency, is more than 100 mJ, which means about 30 mJ per attopulse. With 10% harmonic transport efficiency this results in (3 mJ)/(300 as) $\approx$ 10 TW peak power and a focal spot diameter of 3 μm is sufficient to reach intensity close to 10^{20} W cm^{-2}. In principle, with 10 % Neon concentration and efficient SHHG, close to 1 pC injected charge can be achieved. The larger spot size will result in larger transverse emittance, but the energy spread will be the same.

The parameters of the injected electron bunch are shown in figure 3, which presents the extremely small momentum spread and transverse emittance, which are calculated as: $\sigma_{\rm en} = \sqrt{\bar{\gamma}^2 - \bar{\gamma}^2} m_e c^2$ and $\epsilon_y = \sqrt{(\bar{y^2} - \bar{y}^2)(\bar{p_y^2} - \bar{p_y}^2) - (y\bar{p}_y - \bar{y}\bar{p_y})^2}/(m_e c)$, where the upper bar represents the averaging. It can be seen that the optimum number of pulses is 3 or 4, since at these points in figure 3 an acceptable number electrons get injected while the energy spread is still low. It is important to note that higher number attopulses will increase the energy spread even more, because each attopulse acquires the maximum intensity at different times. Therefore the temporal difference between the firstly injected electrons (by the first attopulse) and lastly injected electrons depends linearly on the number of pulses, which also results in a linear increase of energy difference.

3. Optimal injection and maximum energy gain

Due to the large differences in the wavelengths of injecting and driving pulses the simulation is divided into two steps. First, the ionization injection is modeled with 2 nm mesh resolution (grid size), then these

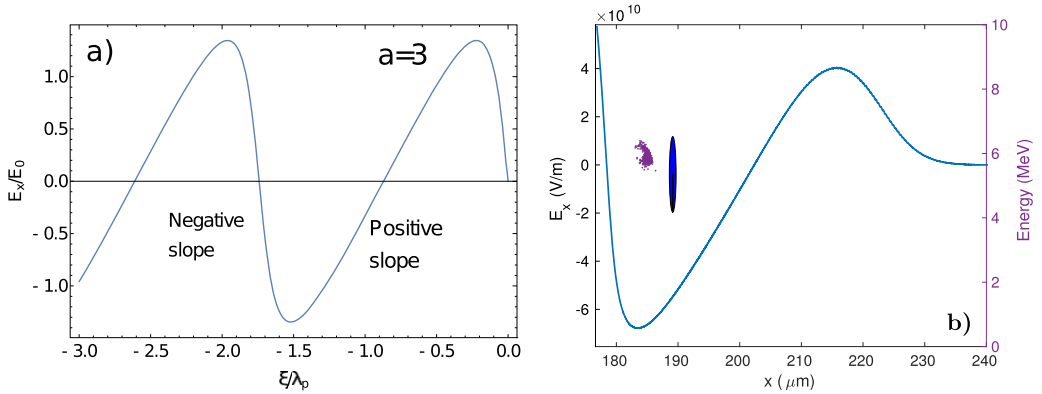

Figure 4. (a) Longitudinal electric field profile in the case of a normalized laser field amplitude of $a = 3$. The electric field is normalized to $E_0 = m_e c\omega_p/e$. (b) Result of the 2D simulation, where the attopulses (shown by blue ellipse) are focused at $x = 100$ μm and are delayed by 85 fs with respect to the peak of the driving pulse. The blue curve represents the longitudinal field profile, while the purple dots are the injected electrons.

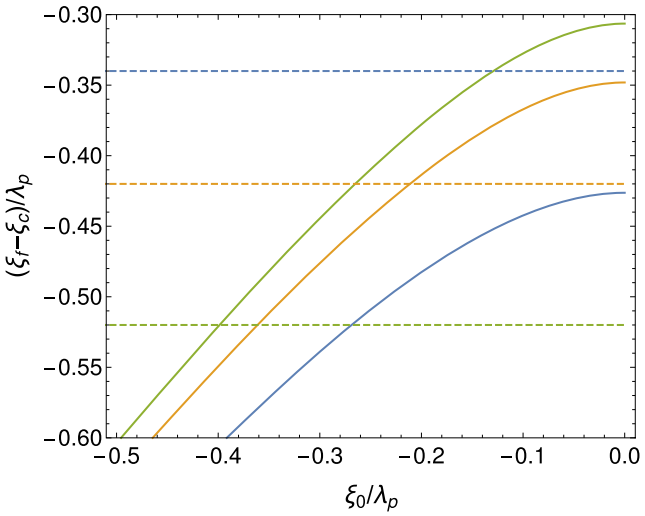

Figure 5. Final position of electrons (full lines) in the ion cavity as a function of focus position of the attopulses for different laser intensities: $a = 1.5$ (blue), $a = 2$ (orange), $a = 2.8$ (green). The dashed lines indicate the position of the peak accelerating field, where its gradient is zero, for the same a values.

electrons are loaded into a larger domain with lower resolution (10 times longer grid size) where the acceleration stage is simulated. The short injection length allows for a very localized injection, therefore the duration of the electron bunches in the wakefield will be also very short. It is worth to note that the ponderomotive potential is on the order of 100 keV, which defines the energy spread in the bunch. The simulation also confirmed this, because right after ionization the maximum energy of electrons is below 1 MeV.

In order to find the optimal position of ionization, or the optimal delay between the driving pulse and attopulse, the electric field profile is modeled in a simplified way. It is well-known that the longitudinal field exhibits positive and negative slopes in separate portions of the ion cavity which gives rise to the spatial energy chirp. The final position of electrons in the moving ion cavity should be between these two region, where the electric field gradient is nearly zero. Our analytical treatment we begin with the self-consistent Poisson equation derived in [44]:

$$k_p^{-2}\frac{\varphi^2\phi}{\varphi\xi^2} = \frac{1+a^2/2}{2(1+\phi^2)} - \frac{1}{2}, \tag{1}$$

where $k_p = (c/\omega_p)^{-1}$ with $\omega_p = \sqrt{e^2 n_e/m_e\epsilon_0}$ being the electron plasma frequency and $\xi = x - v_p t$ with $v_p \approx c$ being the phase velocity of the plasma wave. Further normalization have been applied to the potential, $\phi = e\varphi/m_e c^2$, and to the laser electric field, $a = eE_L/(m_e\omega_L c)$. The solution of equation (1) is shown in figure 4(a), where we see that the electrons should be accelerated near the lowest field value, which is near $\xi = -1.5\lambda_p$ for a normalized vector potential of $a = 3$. In the case of dephasing the positive gradient

of the electric field generates an energy chirp in the bunch and the negative gradient can be used to compensate for the chirp developed during acceleration [17]. In our simulation the group velocity of the laser pulse is very close to the speed of light and the relative shift of the electron bunch should be less than 2 microns after 50 ps with respect to its initial position in the wakefield.

In figure 4(b) the result of a simulation with optimal attopulse delay is presented. The plasma density is $n_e = 6 \times 10^{17}$ cm^{-3}, the pulse duration is $t_L = 50$ fs and the normalized laser field amplitude is $a = 2.8$. One can see that the energy spread of electrons is very low and that they are located near the zero-gradient electric field, which is the key for preserving the quasi-monoenergetic feature of the bunch. Using the one-dimensional relativistic equation of motion the velocity of released electrons evolves as:

$$\frac{v_e}{c} = \left(1 + \frac{1}{G^2(\tau^2/2 + \tau\xi_0 k_p)^2}\right)^{-1/2} \tag{2}$$

where $\tau = \omega_p t$, ξ_0 is the position where the ionization takes place and the positive slope of the electric field is defined as $G = [\epsilon_0/(en_0)](\mathrm{d}E_x/\mathrm{d}x)_+$ and its value is calculated according to equation (1), as in figure 4(a). The position of the attopulse focus (ξ_0) is measured from the center of the ion cavity (ξ_c), i.e. from the point where $E_x = 0$. In order to find their final position (ξ_f) it is sufficient to solve $k_p \mathrm{d}\xi/\mathrm{d}\tau = v_e/c - 1$, which has an asymptotic solution at $\tau \gg 2\pi$. The final positions of the ionized electrons are shown in figure 5 in comparison with the maximum field position, which both depend on a.

The theoretical curves presented in figure 5 give us a hint about the optimal delay between the driving pulse and attopulses. In principle the optimal ξ_0 is found where the full and dashed lines (with the same color) cross each other. In the case of a weak driving pulse (blue lines in figure 5) it is not possible to inject electrons at the right position, only for $\xi_0 > 0$ where the field of the driving pulse would increase dramatically the energy spread. With slightly higher laser intensity we find crossing points, which means that optimal injection is possible. The delay in the simulation presented in figure 4(b) was $\xi_0 = -16\ \mu\mathrm{m} \approx -0.4\lambda_p$, which corresponds to the crossing of the green lines in figure 5.

4. Long distance propagation in a guiding plasma channel

Laser pulses can propagate over many Rayleigh lengths, without significant change in their focal spot radius, in a plasma channel with parabolic density profile if the matched laser spot size is used [45–47]. The upper limit of the efficient acceleration is defined by the dephasing length $L_{\mathrm{dp}} \approx (n_{\mathrm{cr}}/n_0)^{3/2}\lambda_L\sqrt{a_0}$, where $n_{\mathrm{cr}} = m_e\epsilon_0\omega_0^2/e^2$ is the critical density and for our parameters it is $L_{\mathrm{dp}} \approx 10$ cm. Another limiting factor is the energy depletion length $L_{\mathrm{d}} = ct_L(n_{\mathrm{cr}}/n_0)$, which is more than 20 cm in our case. For our proof of principle simulations we chose the following density profile for the channel: $n_e = n_0(1 + (y - y_0)^2/r_{\mathrm{ch}}^2)$, where $r_{\mathrm{ch}} = 19\ \mu$m is the characteristic channel radius. The laser focal spot size at the entrance of the channel has to be matched to the density profile, which is done routinely in the case of low intensity pulses. In our case the relativistic effects have to be also taken into account, thus the evolution of the focal spot radius is governed by the following equation [46]:

$$\frac{\partial^2\rho}{\partial x^2} = \frac{4}{k_0^2\rho^3}\left(1 - \frac{a_0^2}{32}k_p^2 r_{\mathrm{s}}^2 - \frac{\Delta n_0}{\Delta n_c}\rho^4\right), \tag{3}$$

where $\rho = r_{\mathrm{s}}/w_0$ is the spot radius normalized to the initial waist size (w_0), k_0 is the laser wave number, $\Delta n_0 = n_e(w_0) - n_0 = (w_0/r_c)^2 n_0$ and $\Delta n_c = 1/(\pi r_e w_0^2)$ with $r_e = 2.818 \times 10^{-15}$ m. In this equation we neglected the density perturbation generated at the front of the laser pulse, since for our laser parameters it is much smaller than Δn_c. The laser propagation is stable, and the laser spot size does not oscillate, if the right-hand side of equation (3) is zero and $\rho = 1$. This leads to a quadratic equation, where $r_M = w_0$ is the variable, and its solution gives the expression for the matched spot size:

$$r_M^2 = \frac{r_{\mathrm{ch}}^2}{n_0\pi r_e}\left[\left(a_0^4 k_p^4/8^4 + \frac{n_0\pi r_e}{r_{\mathrm{ch}}^2}\right)^{1/2} - (a_0/8)^2 k_p^2\right]. \tag{4}$$

This expression includes the laser intensity as a parameter and for $a_0 \to 0$ we obtain the well-known expression for matched spot size $r_M^4 = r_{\mathrm{ch}}^2/(\Delta n_{\mathrm{ch}}\pi r_e)$, where the channel density depth is $\Delta n_{\mathrm{ch}} = n_0$ in our case. We have tested the acceleration process for the non-relativistic matched spot size, $r_M = 16.1\ \mu$m and for two values including the laser field amplitude, given by equation (4): $r_M = 11.7\ \mu$m and $r_M = 10.8\ \mu$m in the case of $a_0 = 2.8$ and $a_0 = 3.1$, respectively. Several snapshots of the longitudinal electric field along the laser propagation axis are presented in figure 6. One can see that perfect guiding in none of the cases is achieved, since the accelerating field changes due to the change in the laser spot size. However, the

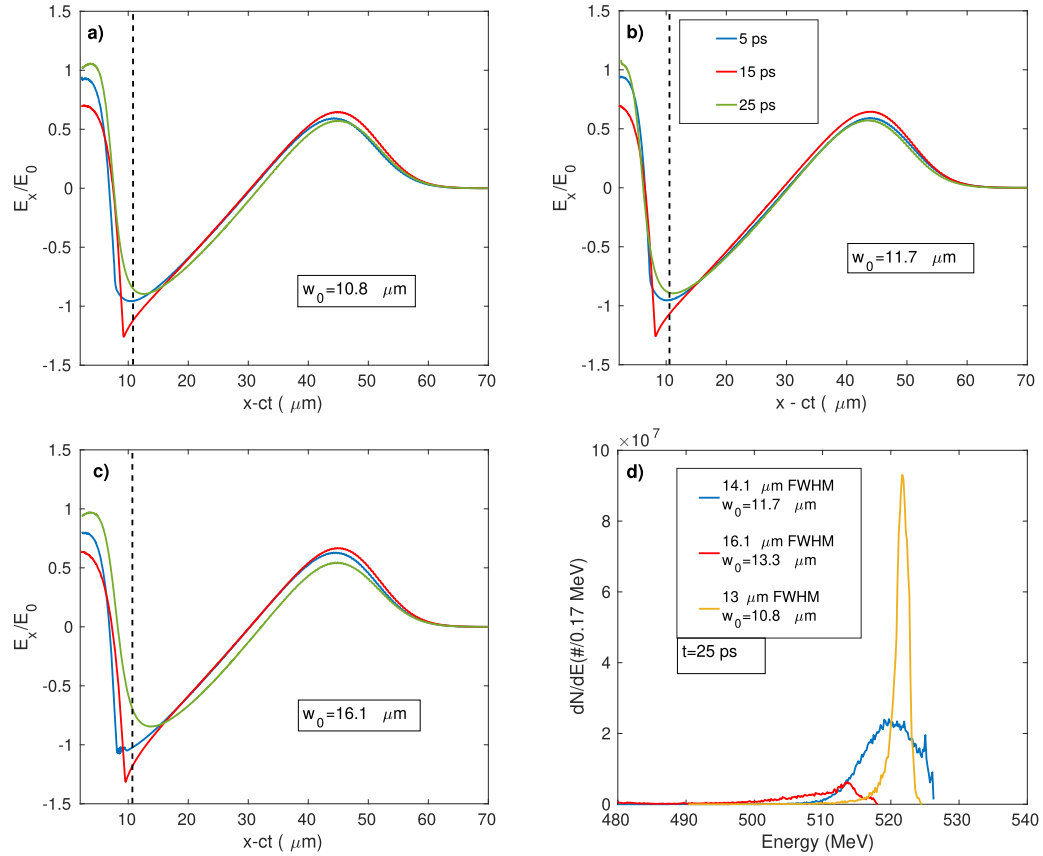

Figure 6. Longitudinal electric field profile along the axis of symmetry of the wakefield at different time instances (a), (b), (c) for all three laser spot sizes mentioned in the text. The vertical dashed line in (a) indicates the position of the center of the electron bunch. In (d) the snapshot of the energy spectra at $t = 25$ ps are shown from the presented simulations.

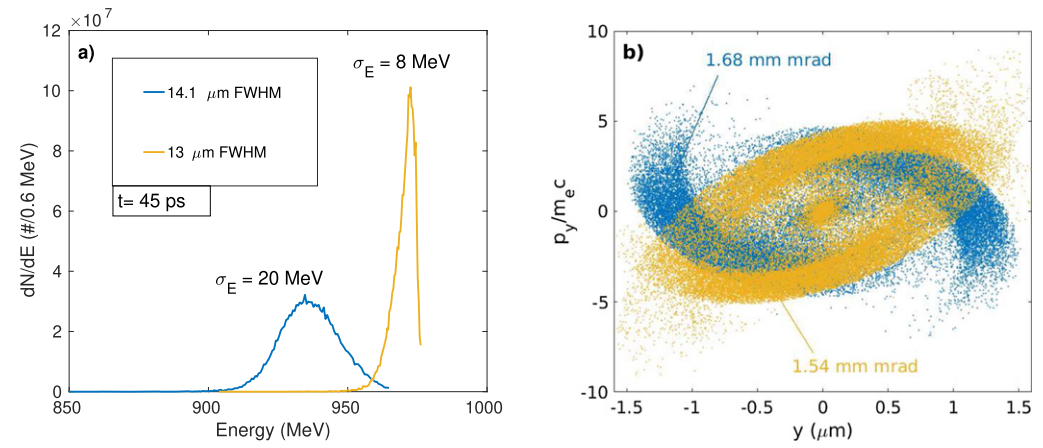

Figure 7. (a) Energy spectra of the injected electrons at a later time of the acceleration and (b) the corresponding transverse phase-space distribution, where the normalized emittance and energy spread are calculated in the same way as in figure 3.

acceleration is improved when the relativistic spot size is used and the best beam quality is obtained for $a_0 = 3.1$ (see yellow line figure 6(d)), which is slightly larger than the actual value at the beginning of the simulation $a_0 = 2.8$.

Although the field oscillates in figure 6(a), the electron energy spread still remains very low. This can be explained by the fact that the electron bunch spends equal time in the negative and positive slope of the field profile, thus on average the energy spread does not increase significantly. At 5 ps the field gradient is zero at the location of the dashed line in figure 6(a), but it becomes positive at 15 ps (red line) and negative at 25 ps (green line). It means that, even if the electric field is not static over time, there exist an optimal oscillation which results in the cancellation of the negative effects of the field gradients. Probably this

phenomenon took place in the case of Ref. [23], where similar mono-energetic electron bunch was observed in a similar 2D simulation, but a detailed explanation was not given. A more elaborated study of the wakefield oscillation in the case of intense laser pulses is beyond the scope of this paper and it remains the subject of a future work. A rigorous investigation in the weakly relativistic regime can be found in reference [47].

The energy spectra and transverse phase-space of electrons at $t = 45$ ps is shown in figure 7(a), which proves that electron bunches with less than 1% energy spread can be generated at the GeV energy level. Both, the initial energy spread and emittance increase during the propagation in the channel by a factor of 40 and 100, respectively. The transverse phase-space distribution, shown in figure 7(b), is very similar for both electron bunches. The geometric emittance (ϵ_y/γ) is below 10^{-3} mm mrad.

5. Conclusions

Proof of principle simulations have been presented for the acceleration of extremely confined (in energy and space) electron bunches at the GeV energy level. The method presented in this work unifies two very distinct areas of laser-plasma physics: the laser-solid interaction, which is responsible for ultra-short coherent radiation emission, and the laser propagation in under-dense plasma, which provides the accelerating structure in a capillary plasma channel. Utilizing the very small ponderomotive potential in the sub-femtosecond pulses electrons with very low energy spread (∼100 keV) can be injected into the wakefield driven by a moderate power (below 100 TW) laser pulse. The first key requirement for avoiding the development of energy chirp is the precise timing between the high-harmonic pulses and the driving laser pulse. The second, and more important, component of a successful setup is a matched laser spot size which enters the plasma channel and undergoes very weak radial oscillations. Finding the best laser spot size is challenging due to the effect of relativistic self-focusing, but we have shown that an optimal spot radius, and thus a minimal oscillation of the wakefield, exist which ensures the low energy spread of electrons during the acceleration. The proposed scheme could be tested in experiments with PW lasers available at different research facilities and could provide a new route toward reproducible generation of ultra-compact GeV electron bunches.

Acknowledgment

We acknowledge KIFÜ/NIIF for awarding us access to HPC resource based in Debrecen, Hungary. The ELI-ALPS project (GINOP-2.3.6-15-2015-00001) is supported by the European Union and co-financed by the European Regional Development Fund. NH acknowledgesPresident International Fellowship Initiative (PIFI) of Chinese Academy of Sciences; International Partnership Program (181231KYSB20170022) of CAS; Inter-Governmental Science and Technology Cooperation of MOST.

Data availability statement

The data that support the findings of this study are available upon reasonable request from the authors.

ORCID iDs

Zsolt Lécz https://orcid.org/0000-0001-5968-8012

References

[1] Leemans W P, Nagler B, Gonsalves A J, Tóth C, Nakamura K, Geddes C G R, Esarey E, Schroeder C B and Hooker S M 2006 GeV electron beams from a centimetre-scale accelerator *Nat. Phys.* **2** 696
[2] Hafz N A M *et al* 2008 Stable generation of GeV-class electron beams from self-guided laser-plasma channels *Nat. Photon.* **2** 571
[3] Wang X *et al* 2013 Quasi-monoenergetic laser-plasma acceleration of electrons to 2 GeV *Nat. Commun.* **4** 1988
[4] Leemans W *et al* 2014 Multi-GeV electron beams from capillary-discharge-guided subpetawatt laser pulses in the self-trapping regime *Phys. Rev. Lett.* **113** 245002
[5] Gonsalves A J *et al* 2019 Petawatt laser guiding and electron beam acceleration to 8 GeV in a laser-heated capillary discharge waveguide *Phys. Rev. Lett.* **122** 084801
[6] Mirzaie M *et al* 2015 Demonstration of self-truncated ionization injection for GeV electron beams *Sci. Rep.* **5** 14659
[7] Yoon J W, Jeon C, Shin J, Lee S K, Lee H W, Choi I W, Kim H T, Sung J H and Nam C H 2019 Achieving the laser intensity of 55 × 1022 W cm^{-2} with a wavefront-corrected multi-PW laser *Opt. Express* **27** 20412–20

[8] Rimantas B et al 2019 53 W average power CEP-stabilized OPCPA system delivering 5.5 TW few cycle pulses at 1 kHz repetition rate Opt. Express 25 5797
[9] Tajima T and Dawson J M 1979 Laser electron accelerator Phys. Rev. Lett. 43 267
[10] Esarey E, Schroeder C B and Leemans W P 2009 Physics of laser-driven plasma-based electron accelerators Rev. Mod. Phys. 81 1229
[11] Umstadter D, Kim J K and Dodd E 1996 Laser injection of ultrashort electron pulses into wakefield plasma waves Phys. Rev. Lett. 76 2073
[12] Esarey E, Hubbard R F, Leemans W P, Ting A and Sprangle P 1997 Electron injection into plasma wakefields by colliding laser pulses Phys. Rev. Lett. 79 2682
[13] Faure J, Rechatin C, Norlin A, Lifschitz A, Glinec Y and Malka V 2006 Controlled injection and acceleration of electrons in plasma wakefields by colliding laser pulses Nature 444 737
[14] Bulanov S, Naumova N, Pegoraro F and Sakai J 1998 Particle injection into the wave acceleration phase due to nonlinear wake wave breaking Phys. Rev. E 58 R5257
[15] Suk H, Barov N, Rosenzweig J B and Esarey E 2001 Plasma electron trapping and acceleration in a plasma wake field using a density transition Phys. Rev. Lett. 86 1011
[16] Geddes C et al 2008 Plasma-density-gradient injection of low absolute-momentum-spread electron bunches Phys. Rev. Lett. 100 215004
[17] Wang W et al 2016 High-Brightness high-energy electron beams from a laser wakefield accelerator via energy chirp control Phys. Rev. Lett. 117 124801
[18] Chen M, Sheng Z-M, Ma Y-Y and Zhang J 2006 Electron injection and trapping in a laser wakefield by field ionization to high-charge states of gases J. Appl. Phys. 99 056109
[19] Pak A et al 2010 Injection and trapping of tunnel-ionized electrons into laser-produced wakes Phys. Rev. Lett. 104 025003
[20] Yu L-L et al 2014 Two-color laser-ionization injection Phys. Rev. Lett. 112 125001
[21] Xu X L et al 2014 Low emittance electron beam generation from a laser wakefield accelerator using two laser pulses with different wavelengths Phys. Rev. Spec. Top. 17 061301
[22] Zeng M, Luo J, Chen M, Mori W B, Sheng Z-M and Hidding B 2016 High quality electron beam acceleration by ionization injection in laser wakefields with mid-infrared dual-color lasers Phys. Plasmas 23 063113
[23] Cho M H 2018 Controlled electron injection facilitated by nanoparticles for laser wakefield acceleration Sci. Rep. 8 16924
[24] Aniculaesei C et al 2019 Proof-of-Principle experiment for nanoparticle-assisted laser wakefield electron acceleration Phys. Rev. Applied 12 044041
[25] Swanson K K et al 2017 Control of tunable, monoenergetic laser-plasma-accelerated electron beams using a shock-induced density downramp injector Phys. Rev. Accel. Beams 20 051301
[26] Schmid K et al 2010 Density-transition based electron injector for laser driven wakefield accelerators Phys. Rev. Spec. Top. 13 091301
[27] Golovin G et al 2015 Tunable monoenergetic electron beams from independently controllable laser-wakefield acceleration and injection Phys. Rev. Spec. Top. 18 011301
[28] Banerjee S et al 2013 Stable, tunable, quasimonoenergetic electron beams produced in a laser wakefield near the threshold for self-injection Phys. Rev. Spec. Top. 16 031302
[29] Schmid K et al 2009 Few-cycle laser-driven electron acceleration Phys. Rev. Lett. 102 124801
[30] Martinez A et al 2015 Wakefield-induced ionization injection in beam-driven plasma accelerators Phys. Plasmas 22 093107
[31] Manahan G G et al 2017 Single-stage plasma-based correlated energy spread compensation for ultrahigh 6D brightness electron beams Nat. Commun. 8 15705
[32] Hidding B et al 2012 Ultracold electron bunch generation via plasma photocathode emission and acceleration in a beam-driven plasma blowout Phys. Rev. Lett. 108 035001
[33] Xi Y et al 2013 Hybrid modeling of relativistic underdense plasma photocathode injectors Phys. Rev. Spec. Top. 16 031303
[34] von der Linde D and Rzàzewski K 1996 High-order optical harmonic generation from solid surfaces Appl. Phys. B 63 499
[35] Spence D J, Butler A and Hooker S M 2001 First demonstration of guiding of high-intensity laser pulses in a hydrogen-filled capillary discharge waveguide J. Phys. B: At. Mol. Opt. Phys. 34 4103–12
[36] Spence D J, Butler A and Hooker S M 2003 Gas-filled capillary discharge waveguides J. Opt. Soc. Am. B 20 138
[37] Watts I et al 2002 Dynamics of the critical surface in high-intensity laser-solid interactions: modulation of the XUV harmonic spectra Phys. Rev. Lett. 88 155001
[38] Tsakiris G D, Eidmann K, Meyer-ter-Vehn J and Krausz F 2006 Route to intense single attosecond pulses New J. Phys. 8 19
[39] Lécz Z and Andreev A 2018 Enhancement of high harmonic generation by multiple reflection of ultrashort pulses J. Opt. Soc. Am. B 35 A49
[40] Keldysh L V 2017 Multiphoton ionization by a very short pulse Phys.-Usp. 60 1187
[41] Keldysh L V 1965 Ionization in the field of a strong electromagnetic wave Sov. Phys. JETP 20 5 1307
Keldysh L V 1964 Zh. Eksp. Teor. Phys. 47 1945
[42] Ammosov M V, Delone N B and Krainov V P 1986 Tunnel ionization of complex atoms and of atomic ions in an alternating electromagnetic field Sov. Phys. JETP 64 1191–4
[43] Arber T D et al 2015 Contemporary particle-in-cell approach to laser-plasma modelling Plasma Phys. Control. Fusion 57 113001
[44] Bulanov S V, Inovenkov I N, Kirsanov V I, Naumova N M and Sakharov A S 1992 Nonlinear depletion of ultrashort and relativistically strong laser pulses in an underdense plasma Phys. Fluids B 4 1935
[45] Mori W B 1997 The physics of the nonlinear optics of plasmas at relativistic intensities for short-pulse lasers IEEE J. Quantum Electron. 33 1942
[46] Esarey E, Sprangle P, Krall J and Ting A 1997 Self-focusing and guiding of short laser pulses in ionizing gases and plasmas IEEE J. Quantum Electron. 33 1879
[47] Benedetti C, Schroeder C B, Esarey E and Leemans W P 2012 Quasi-matched propagation of ultra-short, intense laser pulses in plasma channels Phys. Plasmas 19 053101